Tunneling Magnetothermopower in Magnetic Tunnel Junction Nanopillars

N. Liebing,[1] S. Serrano-Guisan,[1,*] K. Rott,[2] G. Reiss,[2] J. Langer,[3] B. Ocker,[3] and H. W. Schumacher[1]

[1]*Physikalisch-Technische Bundesanstalt, Bundesallee 100, D-38116 Braunschweig, Germany*

[2]*University of Bielefeld Department of Physics, Universitätsstrasse 25, 33615 Bielefeld, Germany*

[3]*Singulus AG, Hanauer Landstrasse 103, D-63796 Kahl am Main, Germany*

(Received 4 April 2011; published 17 October 2011)

We study tunneling magnetothermopower (TMTP) in CoFeB/MgO/CoFeB magnetic tunnel junction nanopillars. Thermal gradients across the junctions are generated by an electric heater line. Thermopower voltages up to a few tens of μV between the top and bottom contact of the nanopillars are measured which scale linearly with the applied heating power and hence the thermal gradient. The thermopower signal varies by up to 10 μV upon reversal of the relative magnetic configuration of the two CoFeB layers from parallel to antiparallel. This signal change corresponds to a large spin-dependent Seebeck coefficient of the order of 100 μV/K and a large TMTP change of the tunnel junction of up to 90%.

DOI: 10.1103/PhysRevLett.107.177201 PACS numbers: 85.80.Lp, 75.76.+j, 85.30.Mn, 85.75.Dd

Transport coefficients in ferromagnetic materials are spin dependent [1]. The giant [2] and the tunneling [3] magnetoresistance (TMR) are the most prominent examples of spin-dependent electronic transport. Their discovery boosted spintronics [4] with important applications, e.g., in data storage. While spintronics relies on spin-dependent charge transport also spin-dependent heat transport can become important when, e.g., a high current density in magnetic nanodevices creates a significant temperature gradient. The combination and coupling of heat, charge, and spin currents in magnetic nanostructures has recently opened a highly active line of research now referred to as spin caloritronics [5] with important discoveries such as the spin-Seebeck effect [6] or thermally driven spin injection [7]. Furthermore, thermal spin transfer torque was predicted to enable highly efficient magnetization reversal in magnetic nanodevices by thermal gradients [8–10] and first experimental evidence has recently been provided [11].

For spintronics CoFeB/MgO/CoFeB magnetic tunnel junctions (MTJ) are one of the most attractive systems as they can be reliably produced by sputter deposition [12] and show very high TMR ratios. The latter results from the half-metallic character of the coherently tunneling Δ_1 states in the ferromagnetic electrodes [13]. With respect to spin caloritronics applications recent *ab initio* studies also predicted very high spin-dependent Seebeck coefficients of 150 μV/K and correspondingly high tunneling magnetothermopower (TMTP) ratios of the MTJ [14]. Furthermore magnon-assisted tunneling might contribute to TMTP especially in nanosized, mesoscopic MTJs [15]. An experimental confirmation of these predictions would strongly impact materials research in the field of spin caloritronics.

Here, we experimentally study TMTP in CoFeB/MgO/CoFeB nanopillars under thermal gradients across the MTJ. We find a strong increase of the thermopower voltage V_{TP} upon reversal of the magnetic configuration of the two CoFeB layers from parallel to antiparallel. The measured increase of V_{TP} up to 10 μV corresponds to large spin-dependent Seebeck coefficients of the order of 100 μV/K and to large TMTP ratios of the MTJ of 90% making this material system a highly attractive candidate for spin caloritronic applications.

The MTJ stacks are sputter deposited in a Singulus NDT Timaris cluster tool on a Si wafer capped with 100 nm SiO_2. The MTJ stack consists of a bottom contact (BC) of 3 nm Ta/90 nm Cu/5 nm Ta, a pinned layer (PL) stack comprising a synthetic antiferromagnet of 20 nm PtMn/2 nm $Co_{60}Fe_{20}B_{20}$/0.75 nmRu/2 nm$Co_{60}Fe_{20}B_{20}$, the 1.5 nm MgO tunnel junction, the free layer (FL) of 3 nm $Co_{60}Fe_{20}B_{20}$, and a top contact of 10 nm Ta/30 nm Cu/8 nm Ru. The completed stack is annealed for 90 min at 360 °C in 1 T field and lithographically patterned into 160×320 nm^2 wide elliptic nanopillars. An electron micrograph of a typical device is shown in Fig. 1(b). Electrical top contacts (TC1-TC3) to the MTJ nanopillars (position of MTJ marked for TC2) are provided by electron beam lithography and lift-off. To apply thermal gradients a 5 μm wide and 70 nm thick Au heater line (HL) is patterned on top of the nanopillar and is separated from the TC by a 160 nm thick Ta_2O_5 dielectric. The 10 μm wide BC line is running underneath the HL. It acts as a heat sink to establish a well-defined temperature gradient across the MTJ. Figure 1(c) sketches a cross section of the contact and layer structure along the dashed line in (b). The nanopillars show single domain magnetization reversal with uniaxial anisotropies between 8 mT $\leq \mu_0 H_k \leq$ 15 mT, TMR ratios between 70% and 140%, and resistance area products of the order of $\sim$17 $\Omega\,\mu$m^2 [16].

We characterize the spin caloric properties of our MTJ nanopillars by magnetothermo electrical measurements. Such measurements have been used to characterize, e.g., magnetic multilayers [17], nanowires [18], and granular

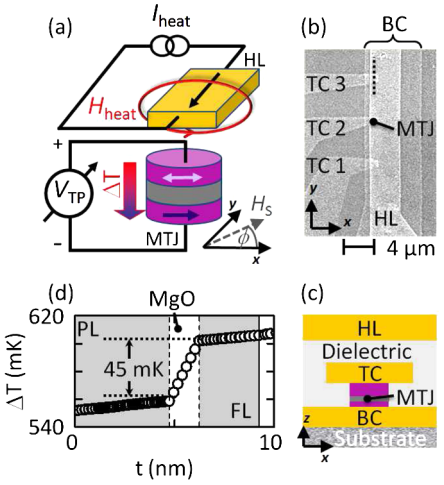

FIG. 1 (color online). (a) Sketch of TMTP setup. A current I_{heat} through the HL creates a temperature gradient across the MTJ and the thermovoltage V_{TP} is measured in in-plane magnetic fields H_S. (b) Electron micrograph of typical device with HL, BC, and top contacts (TC1-TC3) to three nanopillars. The position of the MTJ nanopillar under TC2 is marked. (c) Cross section sketch of contact and layer structure along the dashed line in (b). (d) Simulated temperature for $P_{heat} = 60$ mW in the MTJ as function of thickness t. $t = 0$ corresponds to the bottom of the lowest CoFeB layer.

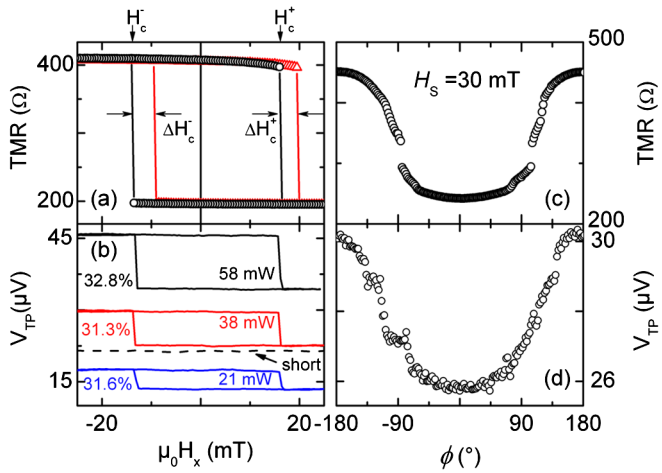

FIG. 2 (color online). Magnetic field dependence of TMR and TMTP of two typical devices MTJ-3 (a),(b) and MTJ-2 (c),(d). (a) Easy axis TMR loop without (black) and with (red) an applied heater current of $I_{heat} = 38$ mA. The TMR switching fields H_C^-, H_C^+ are shifted due to the HL field H_{heat} by ΔH_C^-, ΔH_C^+. (b) Easy axis TMTP loops under applied dc heating powers of $P_{heat} = 21.5$ mW (blue), 37.8 mW (red), and 58.05 mW (black). H_{heat} is compensated. Black dashed line is $V_{TP,short}$ of shorted MTJ. (c) Angular dependent TMR loop for 360° in-plane rotation of static field $\mu_0 H_S = 30$ mT. (d) V_{TP} under same field rotation of (c). V_{TP} is derived under ac excitation with $I_{heat} = 60$ mA, $P_{heat} = 35.15$ mW, and $\pm H_{heat} \approx \pm 6$ mT.

systems [19–21]. The experimental setup is sketched in Fig. 1(a). Static fields up to $\mu_0 H_S = 60$ mT are applied in arbitrary in-plane orientations. Thermal gradients across the MTJ are generated by applying ac or dc heater currents up to $I_{heat} = 60$ mA through the HL while V_{TP} between BC and TC of one of the MTJs is measured. In our measurements a positive V_{TP} corresponds to a positive voltage at the TC. For dc heater currents V_{TP} is measured by a nanovoltmeter. For ac measurements at ac heater frequencies of 10...80 Hz V_{TP} is measured by a lock-in detection at the second harmonic. Note that I_{heat} also generates an easy axis field H_{heat}. For dc measurements H_{heat} is compensated by an external easy axis field H_X whereas for ac measurements such compensation is not possible in our present setup. Hence while ac experiments allow determining V_{TP} with better signal-to-noise ratio the measured $V_{TP}(H_S)$ will always be averaged over an oscillating easy axis field $\pm H_{heat}$ of up to ± 6 mT.

Figure 2(a) shows an easy axis TMR loop (black circles) of one of the MTJ nanopillars (MTJ-3 in Table I). The TMR is measured at a current bias of 100 μA in easy axis fields up to $\mu_0 H_X = \pm 25$ mT. The TMR change of 110% occurs at the reversal from parallel (P) to antiparallel (AP) orientation of the magnetization of the 3 nm thick CoFeB free layer (FL) with respect to the pinned layer (PL) magnetization. In our experiments the PL magnetization is always oriented along the positive x direction. Note that the sharp jumps of the TMR at the coercive fields H_C^- and H_C^+ speak for a single domain reversal behavior of the MTJ FL which is confirmed by well defined switching asteroids in combined easy axis and hard axis fields [not shown; compare Ref. [16], Fig. 1(b) for a typical result].

The second curve in Fig. 2(a) (red triangles) is a TMR loop taken for $I_{heat} = 38$ mA. Here, the effect of H_{heat} is visible and H_C^- and H_C^+ are both offset by about 3.5 mT to positive H_X. Measurements of the coercive field offsets ΔH_C^-, ΔH_C^+ up to $I_{heat} = 60$ mA show a linear scaling of H_{heat} with I_{heat} with a slope of about 0.1 mT/mA (not shown). Note that no significant reduction of H_C with I_{heat} during heating is found in the applied current range and thermally activated reversal can be neglected.

Figure 2(b) shows three typical dc measurements of V_{TP} of the same device. V_{TP} is displayed for heater powers P_{heat} of 21, 38, and 58 mW as function of the easy axis field H_X. H_{heat} is compensated by a static field offset. For all three

TABLE I. Thermoelectric and magnetic properties of the measured MTJs: total anisotropy $\mu_0 H_K$, TMR ratio, and TMTP.

Sample	$\mu_0 H_k$ (mT)	TMR (%)	TMTP (%)
MTJ-1	6	79	32
MTJ-2	8	88	17
MTJ-3	15	110	32
MTJ-4	6.5	134	41
MTJ-5	8	137	30

curves $V_{TP}(P)$ in the P state is lower than $V_{TP}(AP)$ in the AP state with a maximum difference of $\Delta V_{TP} \approx 11\ \mu V$. This yields an average TMTP ratio of the given device of TMTP $= \Delta V_{TP}/V_{TP}(P) \approx 32\%$.

Figure 3(a) shows the typical dependence of $V_{TP}(P,$ AP) on P_{heat}. dc and ac data agree. Measurements were performed at $\mu_0 H_X = \pm 30$ mT in well-defined P and AP configurations. $V_{TP}(P)$, $V_{TP}(AP)$ both scale linearly with P_{heat} and hence with the temperature gradient ΔT_{MTJ} across the MTJ. In Fig. 3(b) the TMTP ratio derived from the same data is plotted vs P_{heat}. The ac data yield a constant TMTP of about 32% (full squares). Here, ac measurements have only been carried out up to $P_{heat} = 34$ mW. Note that the TMTP derived from ac measurements is typically constant over the whole power range displayed in the figure. Also the TMTP derived from dc measurements (open squares) is constant for $P_{heat} \geq 20$ mW with a comparable TMTP $\approx 29\%$. The lower TMTP for $P_{heat} \leq 20$ mW in the dc data can be attributed to an artifact resulting from uncompensated voltage offsets of the nanovoltmeter which are significant at low P_{heat}.

Comparison of our data to the predicted high spin-dependent Seebeck coefficients requires estimating the temperature gradient ΔT_{MTJ} over the MgO MTJ. Therefore the HL resistance R_{HL} is measured as a function of P_{heat} [Fig. 3(c)]. From the increase of R_{HL} with P_{heat} the increase of the HL temperature $\Delta T_{HL}(P_{heat})$ can be derived by $R_{HL} = R_{HL,0}\ (1 + \alpha \cdot \Delta T_{HL})$, where $R_{HL,0}$ is the resistance at room temperature ($P_{heat} = 0$ mW). The HL

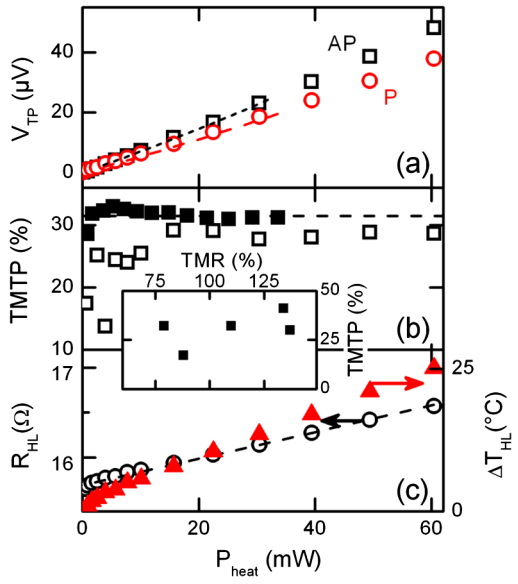

FIG. 3 (color online). (a) V_{TP} as function of P_{heat} for parallel (P, red circles) and antiparallel (AP, black squares) orientation of MTJ-1. dc (symbols) and ac (lines) data agree. (b) TMTP ratio vs P_{heat} for ac (full squares) and dc measurements (open squares). Inset: TMTP vs TMR of the devices of Table I. (c) HL resistance R_{HL} (left scale, circles) and increase of HL temperature ΔT_{HL} (right scale, triangles) as a function of P_{heat}.

temperature coefficient $\alpha = (2.5 \pm 0.3) \times 10^{-3}\ K^{-1}$ was determined using a variable temperature probe station and agrees with literature values obtained for similar geometry [22]. $\Delta T_{HL}(P_{heat})$ is plotted as red triangles in Fig. 3(c). For maximum $P_{heat} = 60$ mW a maximum $\Delta T_{HL} \approx (24 \pm 3)$ K is found. In parallel no change of resistance of the BC line and hence of the BC temperature was observed. ΔT_{HL} thus represents a good estimate of the temperature drop between HL and BC. Based on this the temperature distribution over the nanopillar structure is computed using a commercial finite element solver [23]. We use a two dimensional model of the pillar structure including contacts and insulating layers with thermal material parameters based on literature values [22–25]. The simulations show that the dominant temperature drop occurs across the 160 nm dielectric between HL and TC. In Fig. 1(d) the temperature profile in the nanopillar around the MgO barrier is plotted as function of layer thickness t (z direction). $t = 0$ corresponds to the bottom of the lowest CoFeB layer of the PL. For the given maximum $P_{heat} = 60$ mW one finds a temperature drop across the MgO barrier of $\Delta T_{MTJ} \approx 45$ mK. Based on this one can estimate a spin-dependent Seebeck coefficient of the MTJ of $S_{MTJ} = \Delta V_{TP}/\Delta T_{MTJ} \approx 230\ \mu V/K$ comparable to the predicted value of 150 μV/K [14]. Note, however, that due to the large uncertainty of ΔT_{MTJ} resulting from the simulation (e.g., due to the partial use of bulk values for the thermal conductivity of thin films) only an order of magnitude estimate of S_{MTJ} is feasible.

The above *ab initio* studies of TMTP in MgO based MTJs have also considered the angular dependence of V_{TP} [14]. Figures 2(c) and 2(d) show the measured angular dependence of (c) TMR and (d) V_{TP} for a 360° in-plane rotation of the FL magnetization induced by a rotating static field H_S. V_{TP} is measured with ac heater current. V_{TP} well follows the typical $\cos(\phi - \pi)$ dependence of the TMR [26]. In the TMR two jumps are found around $\phi \approx \pm 90°$ when the free layer magnetization overcomes the hard axis. In V_{TP} these jumps are smoothed out by the uncompensated ac heater field of ± 6 mT. Note that the measured angular dependence does not well follow the theoretical prediction of an almost constant V_{TP} for $|\phi| < \pm 120°$ and a sharp increase near the AP orientation [14]. In contrast both in collinear and tilted field configurations of FL and PL V_{TP} basically follows the field dependence of the TMR.

As listed in Table I our samples reveal TMTP ratios between 17% and 42% and TMR ratios between 79% and 140%. In the inset to Fig. 3(b) the TMTP ratios of the different samples are plotted vs TMR. No significant correlation of the amplitude of TMR and TMTP is found. The TMTP rather seems to scatter around a value of about 31%. Theoretically no close correlation of the TMR and TMTP ratio is expected. While the TMR is sensitive to the density of states (DOS) of the two spin channels at the Fermi level

the TMTP is sensitive to the asymmetry of the DOS [14]. Note that V_{TP} and hence the above TMTP ratios also contain contributions of all nonmagnetic layers of the devices. To determine these the MgO barriers of some devices were shortened by pinholes [27] by application of current stress resulting in a field independent resistance of $\sim 50\ \Omega$. Figure 2(b) also shows $V_{TP,short}$ of the shortened MTJ-3 for $P_{heat} = 58$ mW (dashed line). $V_{TP,short}$ is independent of field confirming the origin of TMTP at the MgO MTJ. Subtracting this background from $V_{TP}(P)$ yields a better estimate of the TMTP contribution of the CoFeB/MgO/CoFeB MTJ. The resulting values of $TMTP_{MTJ} = \Delta V_{TP}/(V_{TP}(P) - V_{TP,short})$ of, e.g., 72% (MTJ-2) and 90% (MTJ-3) are significantly higher than listed in Table I.

Concluding we have observed a large TMTP of up to 90% in MgO/CoFeB MTJs making them a promising candidate for spin caloritronics. S_{MTJ} agrees with *ab initio* predictions while deviations from the predicted angular dependence are found [14]. For all devices $V_{TP}(AP)$ was larger than $V_{TP}(P)$ in agreement with *ab inito* theory and with predictions based on magnon-assisted tunneling [15]. Here, temperature dependent experiments could shine light on the origin of the TMTP as a strong temperature dependence of S_{MTJ} has been predicted by *ab initio* theory [14].

We thank M. Münzenberg and Ch. Heiliger for stimulating discussions. We acknowledge funding by EU IMERA-Plus Grant No. 217257 and by DFG SPP SpinCaT.

Note added.—Recently, similar results based on optical heating have been published [28].

*Corresponding author.
santiago.serrano-guisan@ptb.de

[1] N. F. Mott and H. Jones, *Theory of the Properties of Metal and Alloys* (Oxford University Press, New York, 1953).
[2] M. N. Baibich *et al.*, Phys. Rev. Lett. **61**, 2472 (1988); G. Binasch *et al.*, Phys. Rev. B **39**, 4828 (1989).
[3] M. Jullière, Phys. Lett. A **54**, 225 (1975); J. S. Moodera *et al.*, Phys. Rev. Lett. **74**, 3273 (1995); T. Miyazaki and N. Tezuka, J. Magn. Magn. Mater. **139**, L231 (1995).
[4] I. Zutic *et al.*, Rev. Mod. Phys. **76**, 323 (2004).
[5] G. E. W. Bauer, A. H. MacDonald, and S. Maekawa, Solid State Commun. **150**, 459 (2010).
[6] K. Uchida *et al.*, Nature (London) **455**, 778 (2008); K. Uchida *et al.*, Nature Mater. **9**, 894 (2010); C. M. Jaworski *et al.*, Nature Mater. **9**, 898 (2010).
[7] A. Slachter *et al.*, Nature Phys. **6**, 879 (2010); J-Ch. LeBreton *et al.*, Nature (London) **475**, 82 (2011).
[8] M. Hatami *et al.*, Phys. Rev. Lett. **99**, 066603 (2007).
[9] G. E. W. Bauer *et al.*, Phys. Rev. B **81**, 024427 (2010).
[10] Z. Yuan, S. Wenig, and X. Xia, Solid State Commun. **150**, 548 (2010).
[11] H. Yu *et al.*, Phys. Rev. Lett. **104**, 146601 (2010).
[12] S. S. P. Parkin *et al.*, Nature Mater. **3**, 862 (2004).
[13] S. Yuasa *et al.*, Nature Mater. **3**, 868 (2004).
[14] M. Czerner, M. Bachmann, and C. Heiliger, Phys. Rev. B **83**, 132405 (2011).
[15] E. McCann and V. I. Fal'ko, Appl. Phys. Lett. **81**, 3609 (2002); Phys. Rev. B **66**, 134424 (2002).
[16] S. Serrano-Guisan *et al.*, Phys. Rev. Lett. **101**, 087201 (2008).
[17] L. Gravier *et al.*, Phys. Rev. B **73**, 024419 (2006); **73**, 052410 (2006).
[18] J.-E. Wegrowe *et al.*, IEEE Trans. Magn. **46**, 866 (2010).
[19] J. Shi *et al.*, Phys. Rev. B **54**, 15 273 (1996).
[20] S. Serrano-Guisan *et al.*, Nature Mater. **5**, 730 (2006).
[21] V. A. Belousov *et al.*, J. Exp. Theor. Phys. **105**, 1222 (2007).
[22] B. Stahlmecke and G Dumpich, J. Phys. Condens. Matter **19**, 046210 (2007).
[23] COMSOL Multiphysics. Details on simulation parameters can be found elsewhere. N. Liebing *et al.*, arXiv:1109.5912.
[24] William M. Haynes and David R. Lide, *CRC Handbook of Chemistry and Physics* (CRC Press, Boca Raton, London, New York, 2010), 91th ed.
[25] A. J. Slifka *et al.*, J. Res. Natl. Inst. Stand. Technol. **103**, 357 (1998).
[26] H. Jaffrès *et al.*, Phys. Rev. B **64**, 064427 (2001).
[27] A. Thomas *et al.*, Appl. Phys. Lett. **93**, 152508 (2008).
[28] M. Walter *et al.*, Nature Mater. **10**, 742 (2011).